Pergamon

Int. J. Multiphase Flow Vol. 23, No. 6, pp. 1147–1170, 1997

Printed in Great Britain
PII: S0301-9322(97)00026-8
0301-9322/97 $17.00 + 0.00

DYNAMIC VISUALIZATION OF TWO-PHASE FLOW PATTERNS IN A NATURAL CIRCULATION LOOP

C. C. HSIEH, S. B. WANG and C. PAN

Department of Engineering and System Science, National Tsing Hua University, Hsinchu, Taiwan, 30043, Republic of China

(Received 24 June 1996; in revised form 4 April 1997)

Abstract—Dynamic image processing techniques based on gray level were developed in this study to investigate the variation of two-phase flow patterns in the riser and its interaction with other thermal hydraulic behavior in a natural circulation loop. Four different modes of flows, namely, steady flow with flow rates less than 150 kg/h, periodic flow with a medium magnitude (peak value from 150 to 300 kg/h), periodic flow with a large magnitude (peak value greater than 300 kg/h), and chaotic flow were identified. Single-phase flow and bubbly flow with a very small void fraction (<0.2%) are the two predominant flow patterns in the lower riser, each of which takes about 50% of time, for both steady flow and periodic flow with a medium magnitude. Flow pattern variation for periodic flow with a large magnitude, which mainly takes place during double channel operation, is more complicated. For this mode of flow about 73–83% of time in the lower riser is of single-phase and bubbly flow with a very small void fraction, 4–8% of bubbly flow with a medium to high void fraction, 10–14% of slug flow and 3–8% of churn flow. The later two flow patterns appear periodically with the loop flow rate oscillation. The time percentage for each flow pattern in the lower rise for chaotic flow is quite sensitive to change of experimental conditions. The time percentage for single-phase flow and bubbly flow with a very small void fraction could be as high as 96%, but it could also be as low as 57%; for bubbly flow with a medium to high void fraction, slug flow and churn flow the time percentage ranges from 3 to 15%, 2 to 30% and 0 to 14%, respectively. Such simultaneous measurements of two-phase flow patterns and other thermal hydraulic properties enabled detail investigation into flow mechanism. Moreover, the single factor effect based on the Taguchi experiment matrix was also examined. © 1997 Elsevier Science Ltd.

Key Words: two-phase flow, natural circulation, image processing, flow visualization

1. INTRODUCTION

Two-phase natural circulation loops have many industrial applications, e.g. chemical processes using thermosiphon reboiler, microelectronics cooling, waste heat recovery and nuclear reactors. This is primarily because of their high heat transfer capability, simplicity and passive nature. The density difference between the two-phase mixture in the heater/riser section and the single-phase liquid in the downcomer region is the primary driving force for loop fluid flow. The loop mass flow rate results from the delicate balance between the gravity head available due to downcomer and various pressure losses in the loop. The two-phase parts of these pressure losses are strong functions of void fraction, which, in turn, influences significantly the two-phase flow pattern. In particular, the dynamics of a two-phase natural circulation loop may be significantly associated with the dynamic change of two-phase flow pattern or vice versa.

Although there are extensive experimental studies on two-phase natural circulation loops (Jain *et al.* 1966; Chexal and Bergles 1973; Fukuba and Kobori 1979; Lee and Ishii 1990; Delmastro *et al.* 1991; Aritomi *et al.* 1992; Kyung and Lee 1994; Wu *et al.* 1996), detail investigations into the relationship between loop thermal hydraulic behavior and two-phase flow patterns are quite limited. Early in the 1970s, Chexal and Bergles (1973) investigated two-phase flow instabilities in a low pressure natural circulation loop, which simulates a vertical thermosiphon used in the chemical process industry. Several different types of instabilities were reported with a brief description of flow pattern in some of these regions. For example, periodic large bubble formation at the exit was identified for a region with very low heat fluxes and a wide range of inlet subcooling.

Aritomi *et al.* (1992) explored transient behavior of natural circulation in boiling two-phase flow to simulate the startup process in a natural circulation boiling water reactor. They found that the formation of a large bubble covering the entire flow cross section (slug flow) is the necessary condition for geysering to occur. A flow pattern map was subsequently constructed for a single-channel loop in the plane of inlet velocity versus heat flux. It was evident that such a large bubble appears only under saturated conditions and at inlet velocities lower than 0.3 m/s.

Fairholm *et al.* (1991) used a real-time neutron radiography system to study the flow pattern in a vertical two-phase natural circulation loop with air flow in the test section as the driving force. With the employment of image processing techniques and a neutron radiography system, they were able to identify the flow pattern in an opaque tube.

Recently, Kyung and Lee (1994) studied experimentally the flow behavior in an open two-phase natural circulation loop using Freon-113. At low heat fluxes periodic circulation was reported. They described qualitatively that the periodic circulation is characterized by the sequential occurrence of single-phase, bubbly, slug and churn flows in the riser section. At higher heat fluxes Kyung and Lee found that the flow pattern at the riser section becomes mainly churn or wispy–annular flow and the flow is steady. At even higher heat fluxes, the so-called density wave oscillations appear and the flow pattern in the riser changes from churn flow to wispy–annular flow to annular flow and then back to churn flow in reverse order.

The above brief review of available literature clearly suggests that there is a strong correlation between two-phase flow pattern and thermal hydraulic behavior of a natural circulation loop. However, the descriptions of the flow pattern variation are exclusively qualitative. Therefore, the detailed correlation between flow pattern and loop thermal hydraulic behavior is totally missing. The objective of the present study is to fill this gap with dynamic flow visualization techniques. Transient flow pattern in the riser was recorded and processed using image processing techniques. As a result, the time evolution data of loop flow rate, system pressure, fluid temperature and flow pattern may be compared on the same time basis to explore the detailed interactions between flow pattern and other thermohydraulic properties.

Computer image processing has become a powerful technique to study two-phase flow patterns. As introduced earlier in this section, Fairholm *et al.* (1991) used a real-time neutron radiography system to study flow pattern in a vertical two-phase natural circulation loop with air flow in the test section as the driving force. The pixel intensity was found to be sensitive to the neutron attenuation property of the fluid. Thus, the region with strong variation in pixel intensity is where the gas-liquid interface is located. Therefore, they were able to determine the bubble size. The images obtained were processed and enhanced by image processing techniques, such as frame averaging to reduce noise, image filtering for noise reduction and edge detection and thresholding for image enhancement, etc. Misawa and Anghaie (1991) employed the thresholding technique to determine the void fraction on a zero-gravity boiling channel. By using the thresholding technique, they were able to determine the average bubble size and count the bubble number. Thus, they were able to determine the void fraction in a given experiment. These studies suggest that it is possible to study the detailed structure of two-phase flow using the image processing technique.

2. EXPERIMENTAL DETAILS

2.1. Natural circulation loop

The apparatus employed in this study is a modified one from Wu *et al.* (1996). Figure 1 shows the dimensions and major measuring points of the double channel rectangular natural circulation loop employed. The loop consists essentially of two parallel channels with heated and riser sections, a condenser, a downcomer and upper and lower horizontal sections.

The dual parallel channel section consists of an opaque stainless steel channel and a transparent Pyrex glass channel. The heated part of both channels are annular consisting of an electric heater embedded in a SUS-316 stainless steel tube. The inner diameter of the annulus for the steel channel is 10.6 mm and is 11.2 mm for the Pyrex one. The outer diameter of the annulus is 20.2 mm. In this study only the Pyrex channel is heated by a D.C. power supply. Its maximum power output is 30 kW. The heater in the Pyrex channel has a length of 1.1 m and the upper 0.92 m part is uniformly heated. The wall and the coolant temperatures in the Pyrex channel are measured using

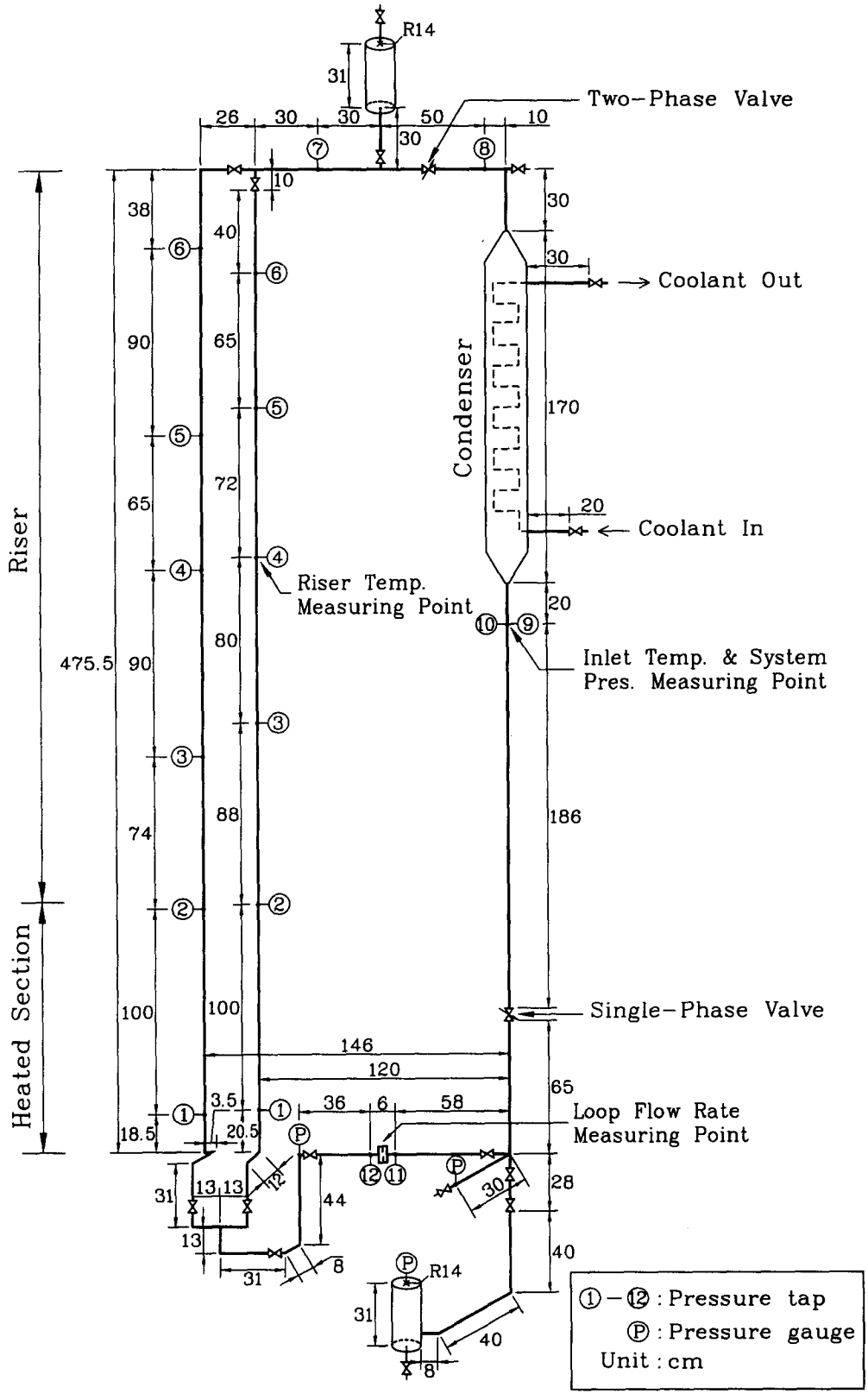

Figure 1. Two-phase natural circulation loop employed in the present study.

K-type thermocouples in three axial locations: 80 mm, 580 mm and 1080 mm from the top of the heated region.

The risers in both channels are adiabatic and well insulated except for two widows in the Pyrex channel for visualization of the flow pattern. The inner diameter of the risers in both channels is 20.2 mm.

The condenser is a shell-tube design having a total height of 1.7 m. The outlet temperature of the primary side working fluid can be controlled by the flow rate and temperature of the cooling water. A storage tank was designed with heaters to regulate the coolant temperature and stabilize the secondary flow rate. The outlet temperature on the primary side from the condenser is considered as the inlet temperature of the heated section.

The downcomer and upper and lower horizontal sections are made of stainless steel with an inner diameter of 20.2 mm. A control valve is located in the downcomer region so that the flow resistance in the single-phase region can be controlled. An orifice flow meter, which is calibrated for both forward and reverse flows, is installed in the lower horizontal section to measure the loop mass flow rate. A pressure regulation tank is also located in the bottom horizontal section to regulate the loop pressure to a desired value. A pressurizer is also installed on the upper horizontal section to study its effect on loop thermal hydraulic behavior. The upper horizontal section also has a control valve to control the flow resistance in the two-phase region.

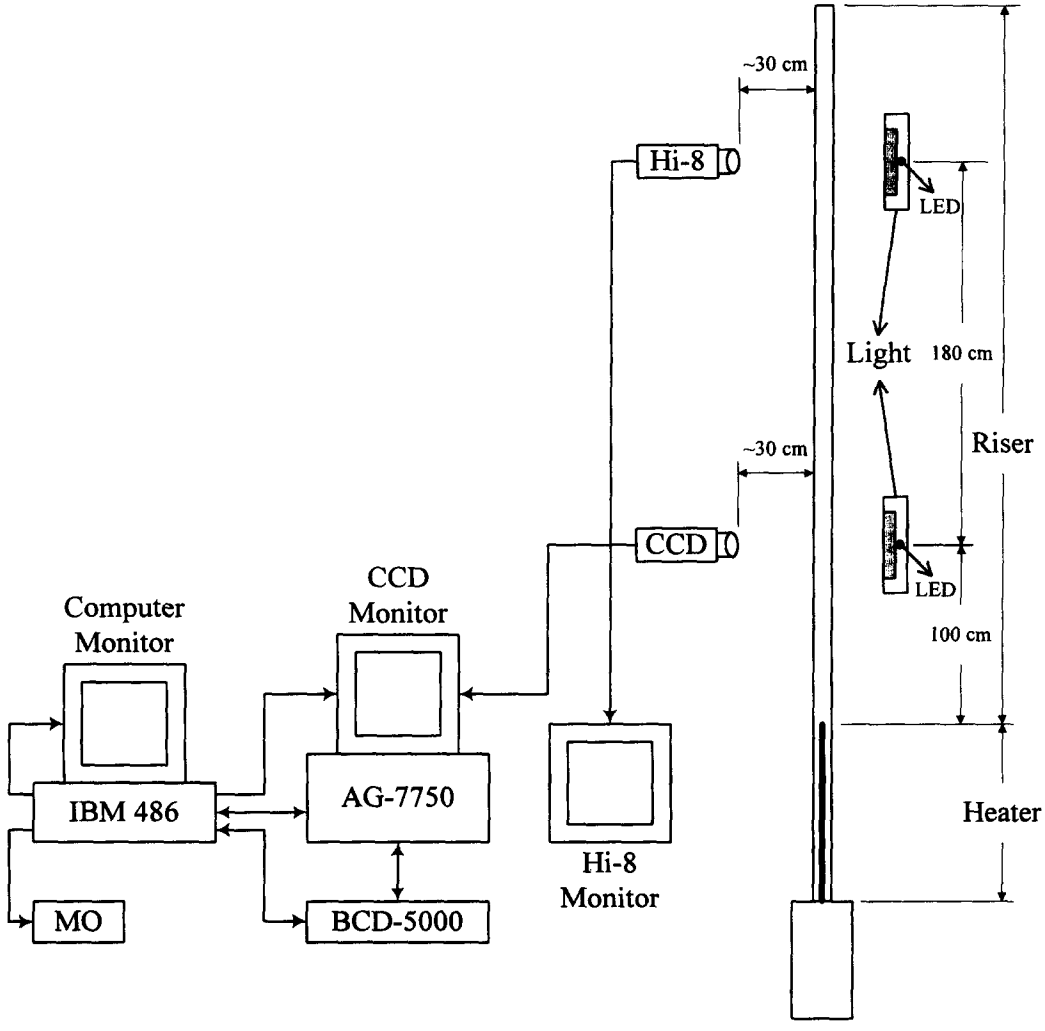

Figure 2. Schematic diagram of flow visualization instrumentation.

The entire loop, except for the heated section and the two windows for flow visualization in the riser of the Pyrex channel, is insulated to minimize heat loss. The pressure drops through each section were measured by differential pressure transducers.

2.2. Flow visualization instrumentation

A schematic diagram of flow visualization instrumentation is shown in figure 2. A Watec WAT-308 CCD camera and a Sony TR-650 8 mm (Hi-8) video camera were installed to obtain the visualization of the transient flow patterns in two axial locations (150 and 280 cm, respectively, from the exit of heated section) in the riser of the Pyrex channel. To obtain best results, a light source, Philips PL18W, was installed in front of each camera but behind the channel. Moreover, the light source was covered with a red transparent plastic paper to produce red light, which has a relatively long wavelength and reduces loss of light due to scattering. In addition, to avoid noise caused by room light, the light path was enclosed by black paper. The shutter speed for both cameras was 1/1500 s which proved to be able to capture the gas–liquid interface clearly.

To synchronize visualization in the two cameras and other system properties, each light source was equipped with a LED and the voltage signals of these two LEDs were also recorded by the data acquisition system. At the beginning of each action, a light and a voltage signal was generated by LEDs. Therefore, the beginning moment of both cameras and the non-image data could be identified accurately and both image and non-image data could be compared in the same time frame.

The analog images captured by the CCD or the Hi-8 were recorded by the Panasonic AG-7750 editor with a speed of 30 frames/s on S-VHS tape. The AG-7750 editor has the ability to freeze, advance or reverse frames without producing significant noise. In the meantime, a time code was

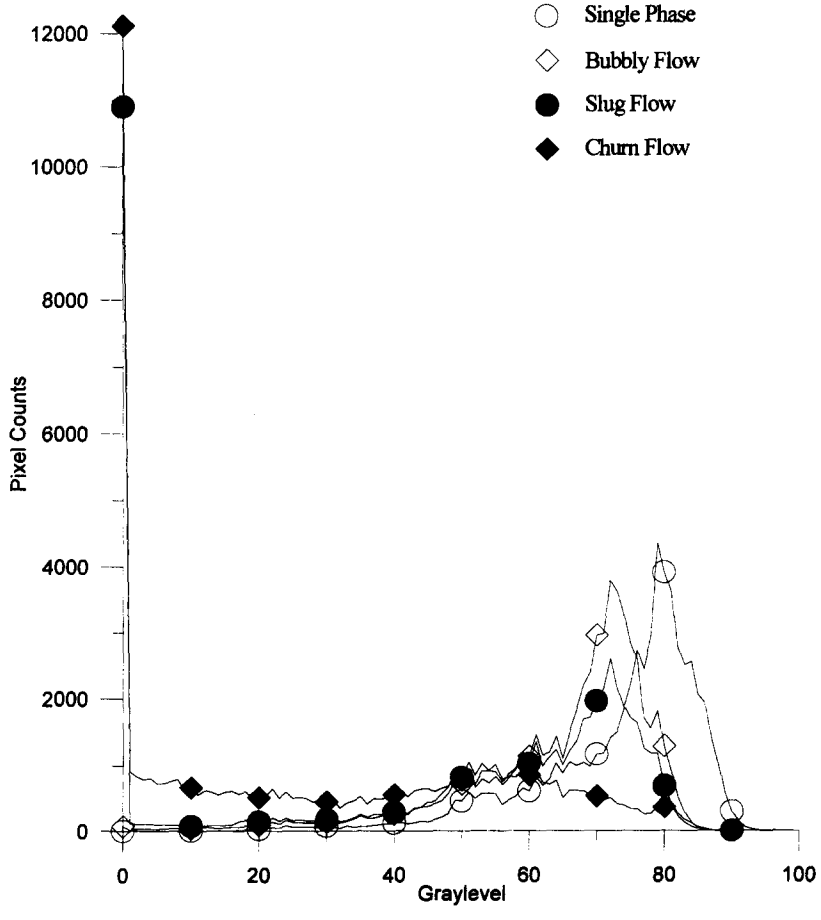

Figure 3. Histograms for various flow patterns.

generated on the video tape controller (BCD-5000). Thus, one might determine the time interval between frames.

The image processing unit includes an IBM 486 personal computer and an image processing card, EPIX, which could convert an analog image to a digital image and store it in a tagged interchange file format on the hard disk of the computer. The flow pattern of each frame could then be identified with the scheme and program developed based on the libraries 4MOBJ and PXIPL in EPIX.

2.3. Data acquisition system

The outputs of thermocouples, flow meters and differential pressure transducers are recorded and analyzed by two data acquisition systems: HP3852 and AR1150A. Both are connected with a personal computer. The former provides 96 channels for recording the data with a sampling rate of 0.5 Hz, while the latter has four channels only and can have a much larger sampling rate. The AR1150A was used for the measurement of the loop mass flow rate, riser fluid temperature, loop system pressure and voltage outputs of the LEDs during the parts of transient and quasi-steady state intervals which are of significant interest for detailed analysis. On the other hand, the HP3852 was on all the time during the experiment.

2.4. Experimental procedure

The experimental procedure employed in this study was different from our previous study (Wu *et al.* 1991). The loop was first operated with two parallel channels, the Pyrex one was heated and

Table 1. Summary of experimental results based on the Taguchi orthogonal experiment matrix

Run no.	Number of channels	Mode of oscillation	Oscillation period (s)	Peak flow rate (kg/h)	Time percentage of each flow pattern in the lower riser (%)			
					Single phase	Bubbly flow	Slug flow	Churn flow
1	2	Chaotic	—	>300	75	7	14	4
	1	Periodic	~28.2, ~8.7	>300	72	6	21	1
2	2	Periodic	~8.5	>300	73	8	12	7
	1	Chaotic	—	>300	64	7	25	4
3	2	Chaotic	—	>300	77	6	12	5
	1	Periodic	~10.5	>300	64	10	20	6
4	2	Steady	—	<150	100	—	—	—
	1	Steady	—	<150	100	—	—	—
5	2	Periodic	~9.9	>300	79	4	10	7
	1	Periodic	~91	150–300	~100	~0	—	—
6	2	Steady	—	<150	100	—	—	—
	1	Steady	—	<150	100	—	—	—
7	2	Periodic	~10.8	150–300	~100	~0	—	—
	1	Periodic	~91	150–300	~100	~0	—	—
8	2	Periodic	~8.9	>300	75	5	11	9
	1	Chaotic	—	>300	79	3	15	3
9	2	Periodic	~11.4	>300	81	5	11	3
	1	Chaotic	—	>300	59	15	21	5
10	2	Periodic	~11.4	>300	83	4	10	3
	1	Chaotic	—	>300	90	3	7	~0
11	2	Chaotic	—	>300	63	6	17	14
	1	Chaotic	—	>300	57	9	28	6
12	2	Periodic	~9.6	>300	77	5	10	8
	1	Chaotic	—	>300	73	4	15	2
13	2	Steady	—	<150	100	—	—	—
	1	Steady	—	<150	100	—	—	—
14	2	Periodic	~9.2	>300	78	4	13	5
	1	Periodic	~82	150–300	~100	~0	—	—
15	2	Periodic	~10.4	>300	78	7	14	1
	1	Chaotic	—	>300	58	10	30	2
16	2	Periodic	~10.2	150–300	93	5	2	~0
	1	Periodic	~91	150–300	100	—	—	—
17	2	Periodic	~9.7	>300	77	5	10	8
	1	Chaotic	—	>300	59	13	23	5
18	2	Chaotic	—	150–300	81	5	12	2
	1	Chaotic	—	150–300	96	2	2	~0

the stainless steel one was unheated. The working fluid, distilled water, was first heated with the top gas relief valve open to boil off the non-condensable gases. During this period, the heating power was approximately linearly increased and automatically controlled by a computer program. The gas relief valve was closed at about a half hour before the specific power was reached. This starting process normally took about 4 h. The loop state was further modulated to the desired average loop pressure and inlet subcooling by adjusting the flow rate and inlet temperature of the secondary cooling water until the steady state or quasi-steady state was reached. Moreover, the gas relief valve might be momentarily opened to adjust the loop pressure. This tuning process typically took 2–3 h. The steady or quasi-steady state for dual channel operation was continued for about 2 h for detail data recording and visualization. Subsequently, both ends of the unheated channel were closed and the loop was operated with a single heated channel. Another modulation process for about 2 h was needed to reach steady state or quasi-steady state operation with a single heated channel. The steady or quasi-steady state also was maintained for two hours for detailed data recording and study before the down load process began. The whole experiment took about 14 h.

Three periods of visualization recording for each camera were conducted for each experiment. Background images were obtained for 5 min during single-phase flow of the starting period and subsequently visualization was conducted for the transient heating process for about 110 min. The steady or quasi-steady state visualization was conducted during the second period. Both cameras were on for another hour after the unheated channel was closed to study the transient behavior for the loop from two-channel to single-channel operation. Steady state video pictures were also taken for the single-channel case during the second steady or quasi-steady operation. Visualization was conducted for another hour after the single-channel steady or quasi-steady operation was ended and down load operation started. Only steady or quasi-steady visualizations are reported in this paper.

The HP 3852 data acquisition system was on all the time during the experiment to keep track of all loop states during the experiment. On the other hand, the other system, the AR1150A, was employed only during part of three visualization periods for data recording with a higher sampling rate. Each of the three sampling periods lasted for 52 min.

3. IMAGE PROCESSING TECHNIQUES

The basic principle of image formation for the various two-phase flow patterns is the deflection of incident light at the interface between vapor and liquid. As a result, a dark region is formed

Table 2

	Factor level						Data film name	
	Inlet temperature (°C)	Heating power (kW)	Upper pressurizer (water level)	Lower pressurizer (water level)	Valve in two-phase flow region (turns of closure)	Valve in single-phase flow region (turns of closure)	Double	Single
1	70	6	Disconnected	Disconnected	0	0	10651204	10651306
2	70	8	High†	High	2½	2½	2064O204	2064O306
3	70	7	Low‡	Low	4¼	4¼	3065E204	3065G306
4	50	6	Disconnected	High	2½	4¼	4064P204	4064P306
5	50	8	High	Low	4¼	0	5064G204	5064G306
6	50	7	Low	Disconnected	0	2½	6064C204	6064C306
7	60	6	High	Disconnected	4¼	2½	7064R204	7064R306
8	60	8	Low	High	0	4¼	8064I204	8064I306
9	60	7	Disconnected	Low	2½	0	90659204	90659306
10	70	6	Low	Low	2½	2½	A064S204	A064S306
11	70	8	Disconnected	Disconnected	4¼	4¼	B064L204	B064L306
12	70	7	High	High	0	0	C064E204	C064E306
13	50	6	High	Low	0	4¼	D064P204	D064P306
14	50	8	Low	Disconnected	2½	0	E064K204	E064K306
15	50	7	Disconnected	High	4¼	2½	F0653204	F0653306
16	60	6	Low	High	4¼	0	G064S204	G064S306
17	60	8	Disconnected	Low	0	2½	H065J204	H064J306
18	60	7	High	Disconnected	2½	4¼	I064D204	I064D306

†High: 20 ± 2 cm. ‡Low: 10 ± 2 cm.
0 turns correspond to a loss coefficient of 0.3.
2½ turns correspond to a loss coefficient of 13.
4¼ turns correspond to a loss coefficient of 480.

representing the vapor-liquid interface. Therefore, different images for various flow patterns will certainly result in significant different histograms as shown in figure 3. Since the images are relatively dark, the gray level for all the images is less than 150. The images for single phase liquid flow and bubbly flow are relatively white due to less light deflection. Therefore, they have very small pixel counts for gray level zero, which represents the darkest level, and have relatively high pixel

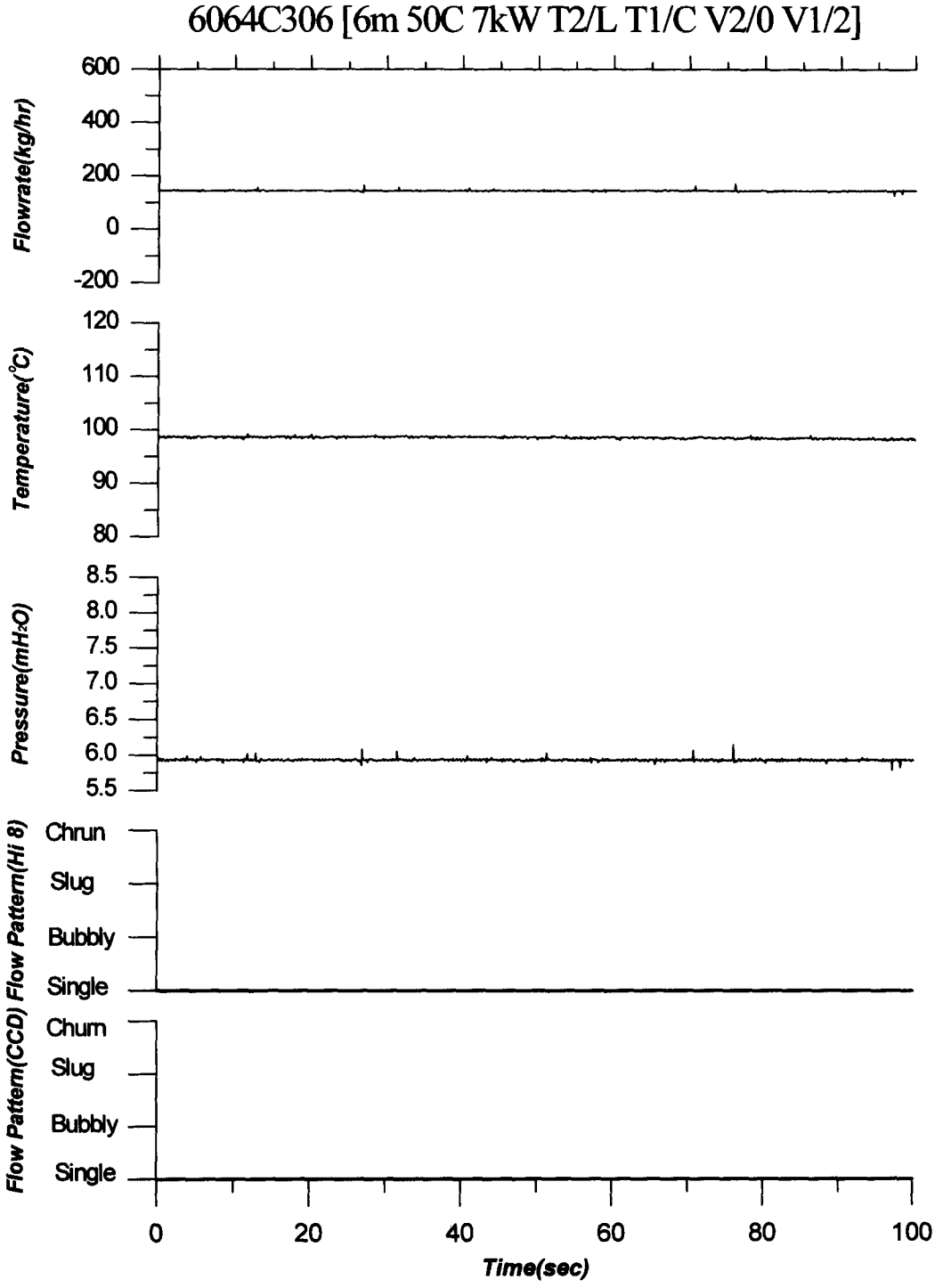

Figure 4. Time evolution of loop mass flow rate, riser fluid temperature and riser flow patterns in upper and lower riser for a typical steady flow. Hi8: upper riser; CCD: lower riser.

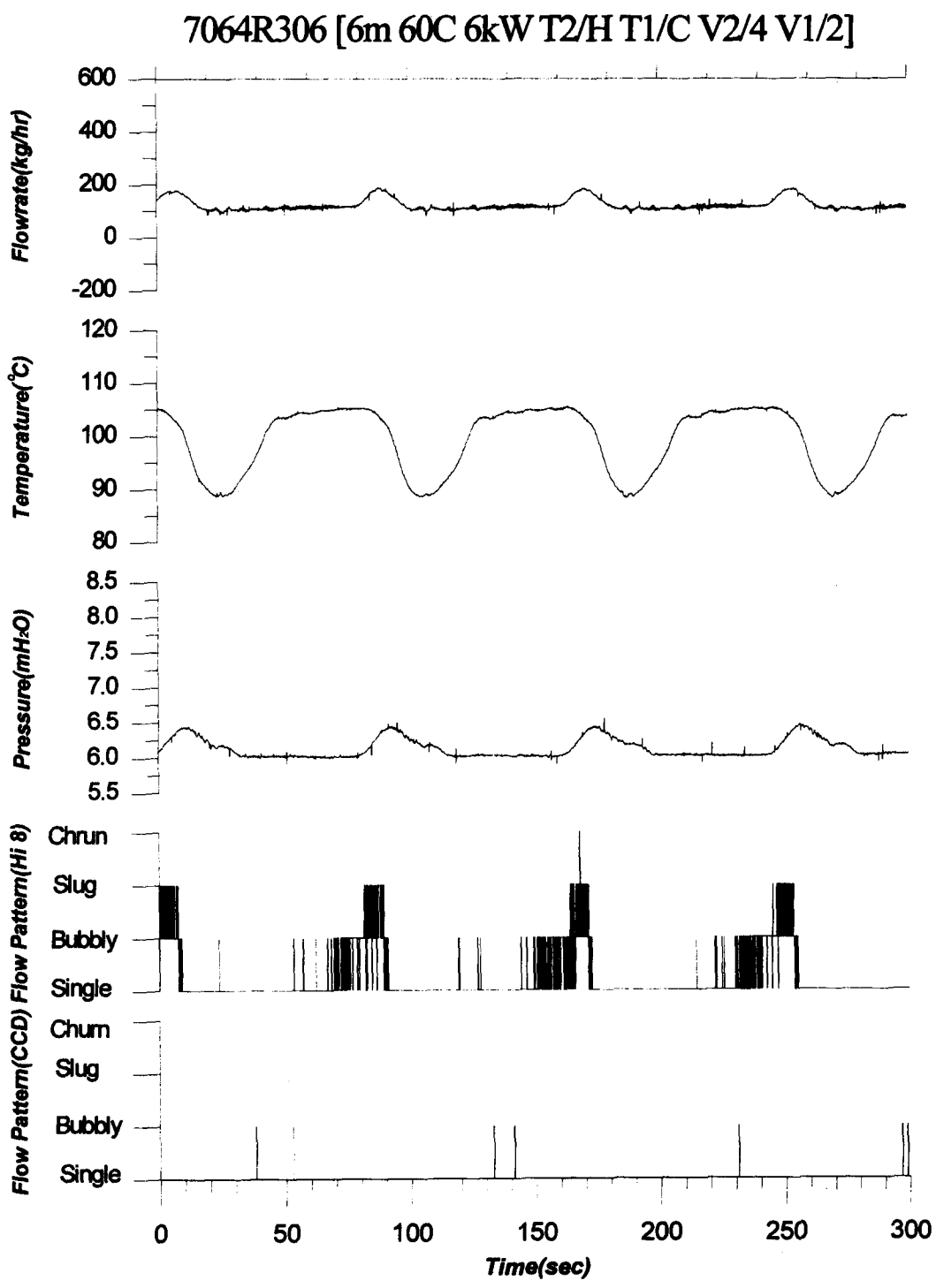

Figure 5. Time evolution in loop mass flow rate, riser fluid temperature, loop pressure and flow patterns in upper and lower riser for a typical periodic flow with a medium magnitude. Hi8: upper riser; CCD: lower riser.

counts for higher gray levels. On the other hand, typical slug and churn flows have very high pixel counts for gray level zero and relatively small counts for large gray levels. Moreover, there is significant difference in gray level distribution among the four different flow patterns observed in the natural circulation loop of this study. This provides a basis for flow pattern identification using the analysis of the histogram from each image.

Four different schemes based on the analysis of histogram have been developed in this study to identify the flow pattern. Two of the four schemes are integral approaches based on both the average gray level and the standard deviation of each histogram. The other two schemes are local approaches based on the gray level distribution without averaging. Histograms for each standard flow pattern of more than 30 images were first obtained and analyzed. The histogram of each image was compared with that for standard images to identify the flow pattern using the four different schemes. An image was assigned to a particular flow pattern based on the 'major vote' principle. However, a different weighting factor was imposed on each scheme to have the best success ratio.

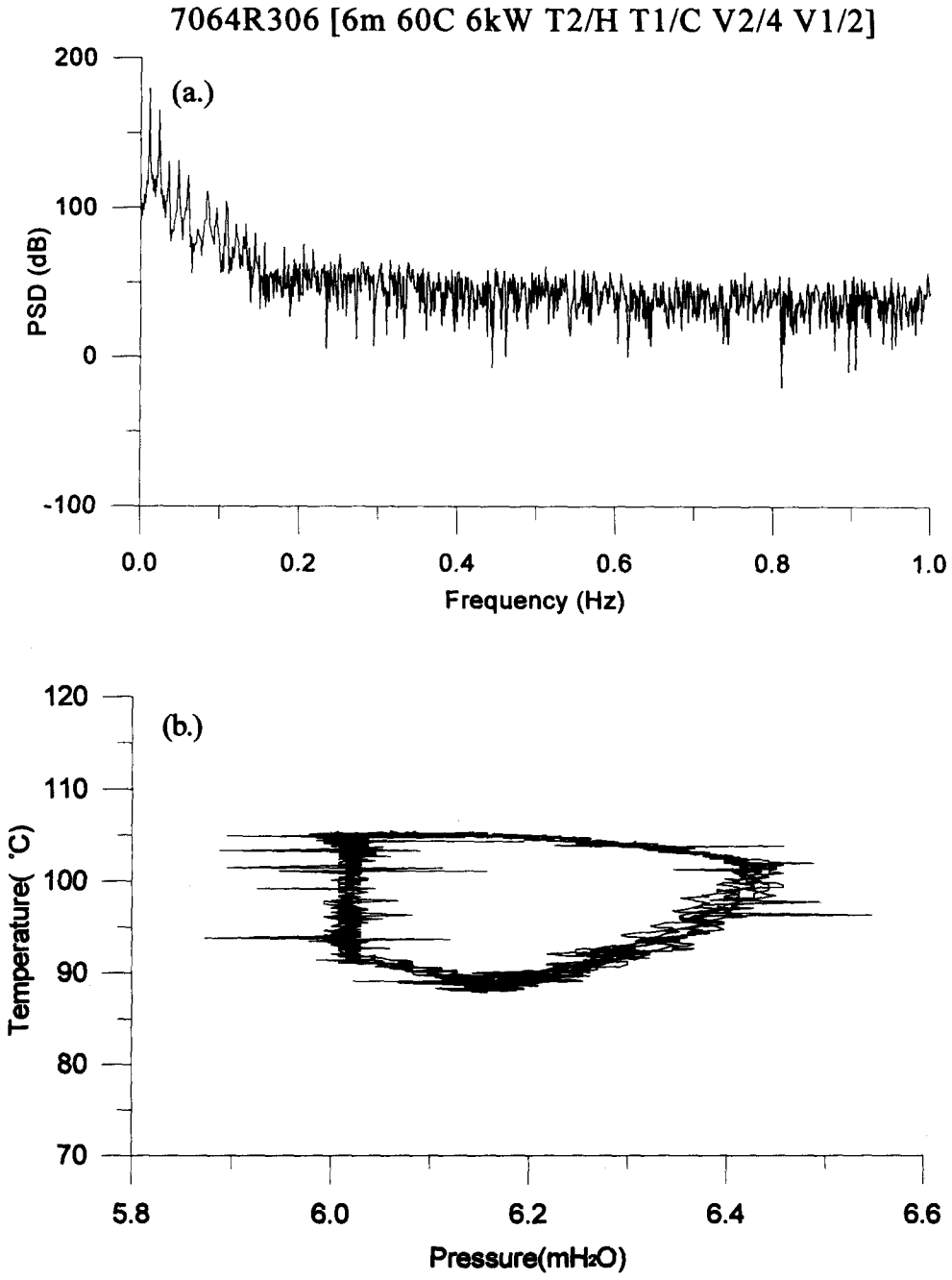

Figure 6. (a) Power spectrum of loop pressure. (b) Phase portrait in the plane of loop pressure and riser fluid temperature for a typical periodic flow with a medium magnitude shown in figure 5.

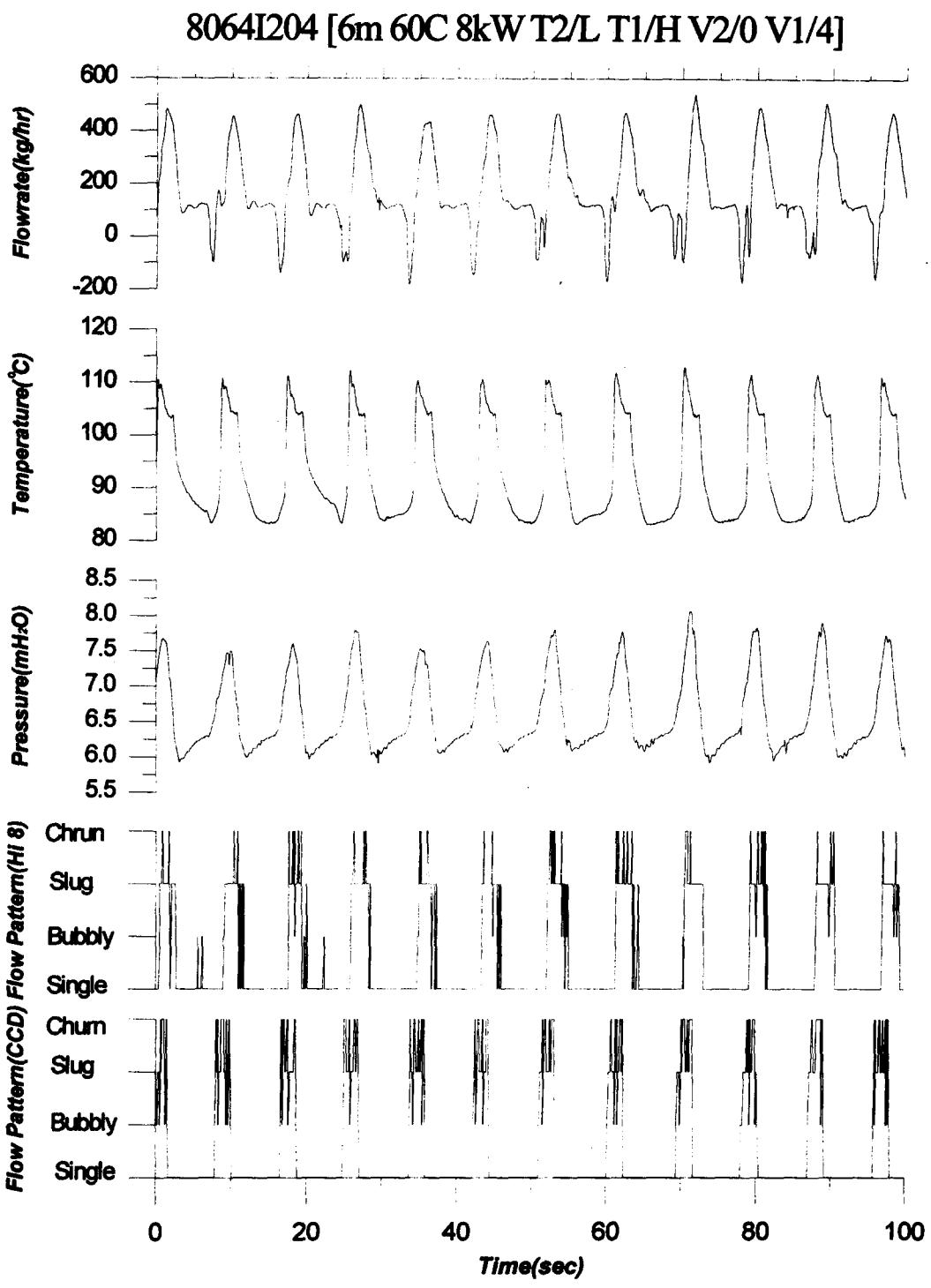

Figure 7. Time evolution of loop mass flow rate, riser fluid temperature, loop pressure and flow patterns in upper and lower riser for a typical periodic flow with a large magnitude. Hi8: upper riser; CCD: lower riser.

Such an approach results in an average success ratio of 94% for the images from CCD, in flow pattern identification with four groups of standard flow patterns, i.e. single phase flow (including bubbly flow with a very small void fraction ($<0.2\%$)), bubbly flow, slug flow and churn flow. Detail descriptions of each scheme and the 'major vote principle' is presented by Hsieh (1996).

4. RESULTS AND DISCUSSION

4.1. Modes of flow and flow pattern

Table 1 summarizes the 18 sets of experimental results obtained in the present study based on the Taguchi orthogonal experimental matrix. Experimental conditions for each set of experiments are listed in table 2. The system gauge pressure was maintained at about 6 mH_2O plus oscillation. The table clearly indicates that there are four different modes of flow prevailing in the natural circulation loop of this study, namely, steady circulation, periodic flow with a medium magnitude (150 < peak value < 300 kg/h), periodic flow with a large magnitude (peak value > 300 kg/h) and chaotic flow.

The steady flow is characterized by the flow rate being smaller than 150 kg/h and the flow pattern is dominated by single-phase flow and bubbly flow with a very low void fraction (<0.2%). This

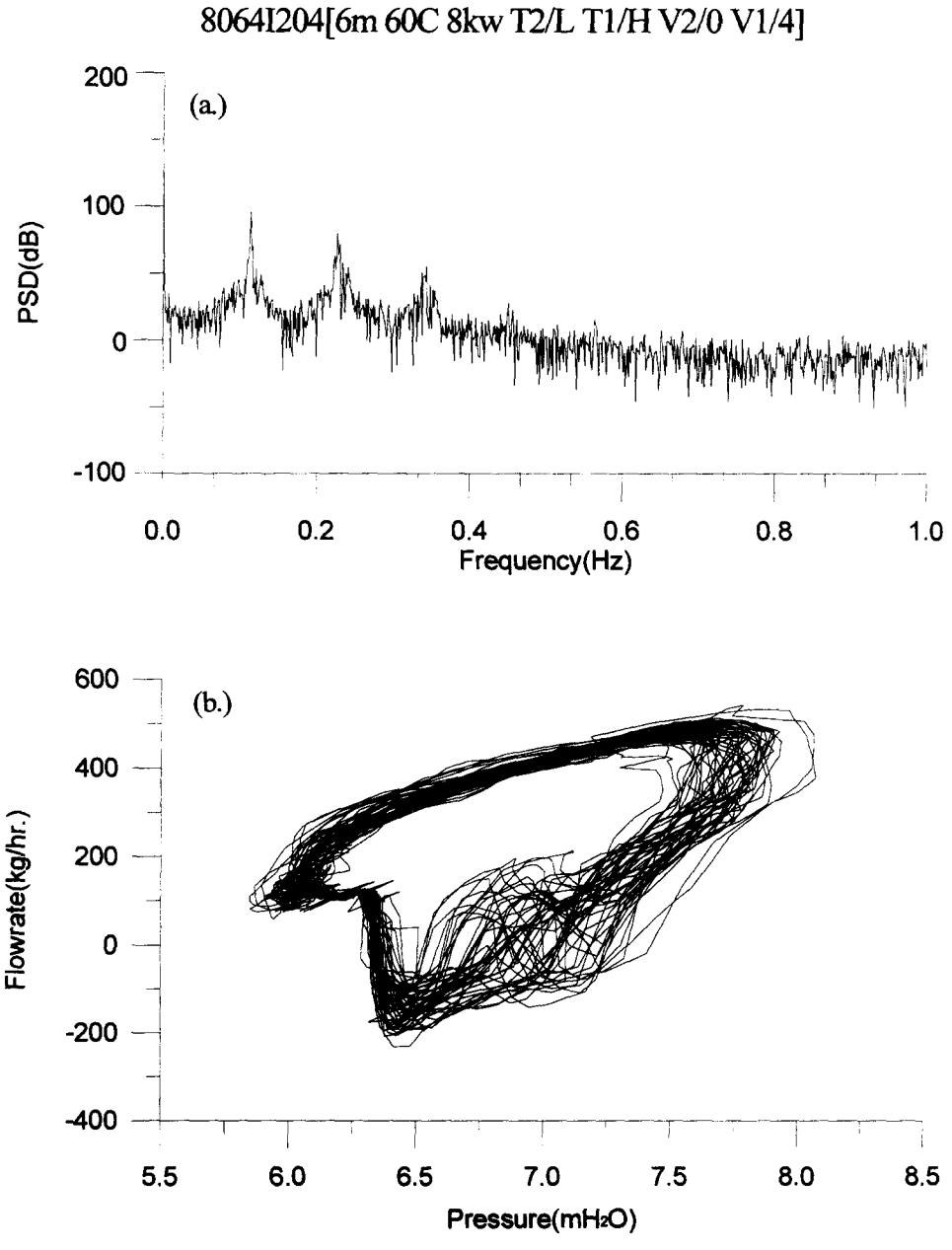

Figure 8. (a)—*Caption opposite.*

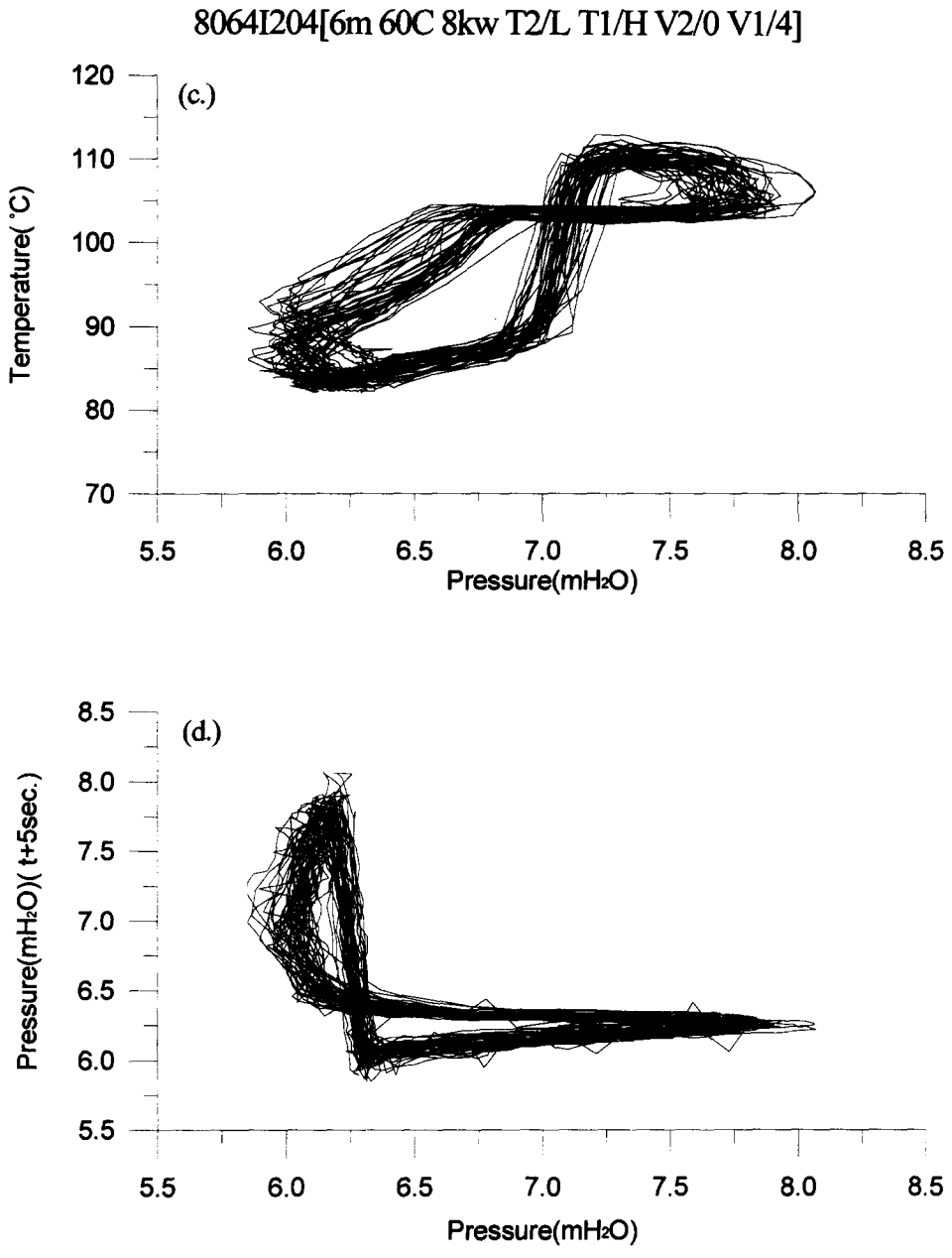

Figure 8. (a) Power spectrum of loop pressure. (b) Phase portrait in the plane of loop pressure and flow rate. (c) Phase portrait in the plane of loop pressure and riser fluid temperature. (d) Pseudo phase portrait of pressure with a delay time of 5 s for a typical periodic flow with a large magnitude shown in figure 7.

kind of bubbly flow with a very low void fraction cannot be effectively distinguished from the single phase flow if only four standard flow patterns are employed. About 50% of single-phase flow identified based on four standard flow patterns can be distinguished as bubbly flow with a very low void fraction if seven groups of flow patterns are employed as standards. In fact, it is because there is little or no void fraction in the riser, that the loop mass flow rate is relatively small. Figure 4 shows the time evolution of the loop mass flow rate, riser fluid temperature, loop pressure and flow patterns in the lower and upper risers. The figure clearly indicates only single phase flow or bubbly flow with a very small void fraction prevails in the riser.

The medium magnitude periodic flow is characterized by peak flow rates ranging from 150 to 300 kg/h. Figure 5 exhibits the time evolution of the loop mass flow rate, riser fluid temperature, loop pressure and flow patterns in the lower and upper riser for a typical case of periodic flow

with a medium magnitude. For this case the flow pattern in the lower riser is also predominated by single-phase flow and bubbly flow with a very low void fraction. The flash in the riser results in the change of flow pattern in the upper riser in which bubbly flow with a relatively high void fraction is formed frequently and slug flow is formed regularly as shown in the figure. A peak in both system pressure and flow rate with a medium magnitude thus follows the appearance of slug flows. This flow rise drives the cool liquid from the entrance to the riser, hence, a reduction in riser fluid temperature follows. It may be said that periodic flow with a medium magnitude is induced by the flash effect in the upper riser. Figure 6(a) and (b) illustrate the power spectrum of loop pressure and the phase portrait based on the riser fluid temperature and loop pressure. This figure demonstrates that the oscillation is indeed periodic.

The periodic flow with a large magnitude is distinguished by peak flow rates being larger than 300 kg/h and the appearance of reversed flow. Table 1 indicates that single-phase flow, or more precisely, single-phase flow and bubbly flow with a very low void fraction, are still the basic flow patterns in the lower riser. The percentage of both patterns together ranges from 73 to 83. The bubbly flow with a medium to high void fraction takes 4–8% of time. The appearance of slug and churn flows in the lower riser is another characteristic of this mode of flow. These two flow patterns take about 12–20% of time.

The correlation between the variation of flow pattern and the oscillations of other physical properties is clearly depicted in figure 7 for periodic flow with a large magnitude. The regular appearance of slug and churn flow in the lower and then upper riser is coincident with the appearance of high loop pressure, riser fluid temperature and it is followed by high mass flow rate. The presence of slug and churn flow suggests a high void fraction in the riser and thus a high loop pressure; a high riser fluid temperature and a high mass flow rate results. Figure 8(a), (b), (c) and (d) exhibit the power spectrum of loop pressure, the phase portrait based on loop mass flow rate

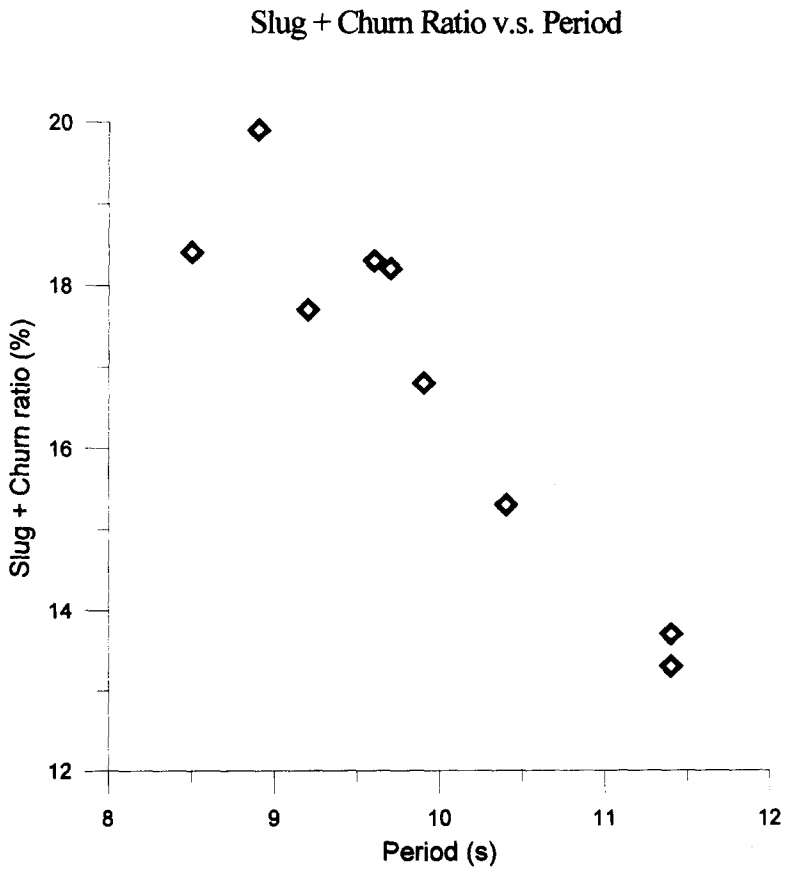

Figure 9. The time percentage of slug and churn flows versus period of oscillation for periodic flow with a large magnitude.

and pressure, the phase diagram based on riser fluid temperature and loop pressure and the pseudo-phase portrait based on loop pressure, respectively. The relatively wide banded phase portraits suggest that the oscillation may be a type of quasi-periodic oscillation. However, the distinguished fundamental peak and its harmonics in the power spectrum, as shown in figure 8(a), confirms that the oscillation is indeed periodic. The relatively wide banded phase portrait is believed

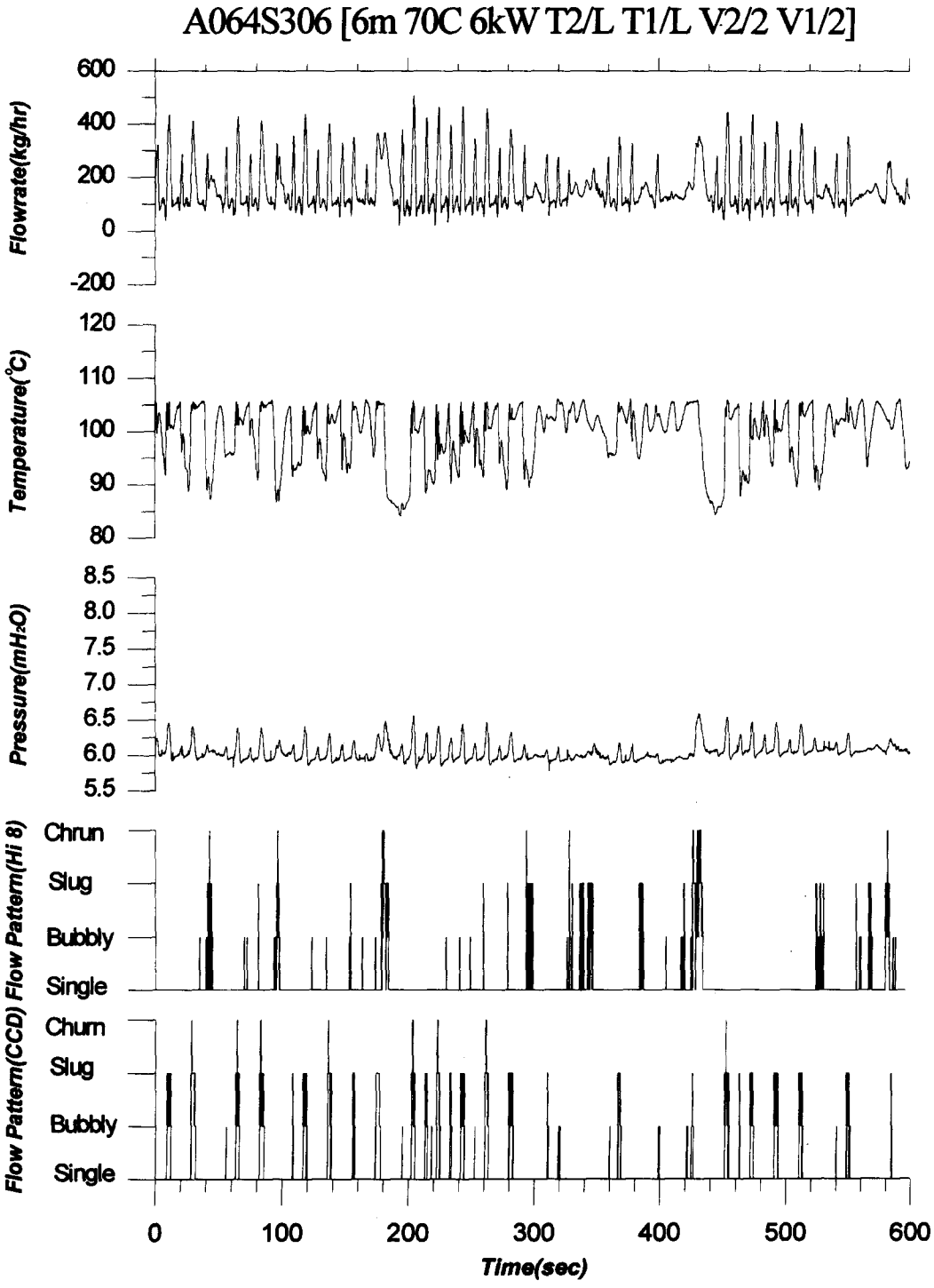

Figure 10. Time evolution of loop mass flow rate, riser fluid temperature, loop pressure and flow patterns in upper and lower riser for a typical chaotic flow. Hi8: upper riser; CCD: lower riser.

to be caused by the large variation of various properties, compared to those for medium magnitude periodic flow, due to complex and fast changing flow pattern.

Another interesting phenomena to be noted is the correlation between the time percentage of slug and churn flow patterns in the lower riser and period of oscillation. Figure 9 indicates that the period of oscillation increases with decrease in time percentage of these two flow patterns. As discussed previously, a higher percentage of slug and churn flow patterns suggests a higher loop mass flow rate. This reduced the time needed for the fluid to circulate around the loop and a shorter period of oscillation results. This is because the oscillation in a close natural circulation loop is associated with multiple feedback between void generation rate, flow pattern change, flow rate, and pressure drop through the boundary conditions that the total pressure drop through the loop must be zero. The transport time of fluid particle will influence the time delay for these feedback mechanisms. Therefore, a shorter period of oscillation follows a shorter transport time of fluid.

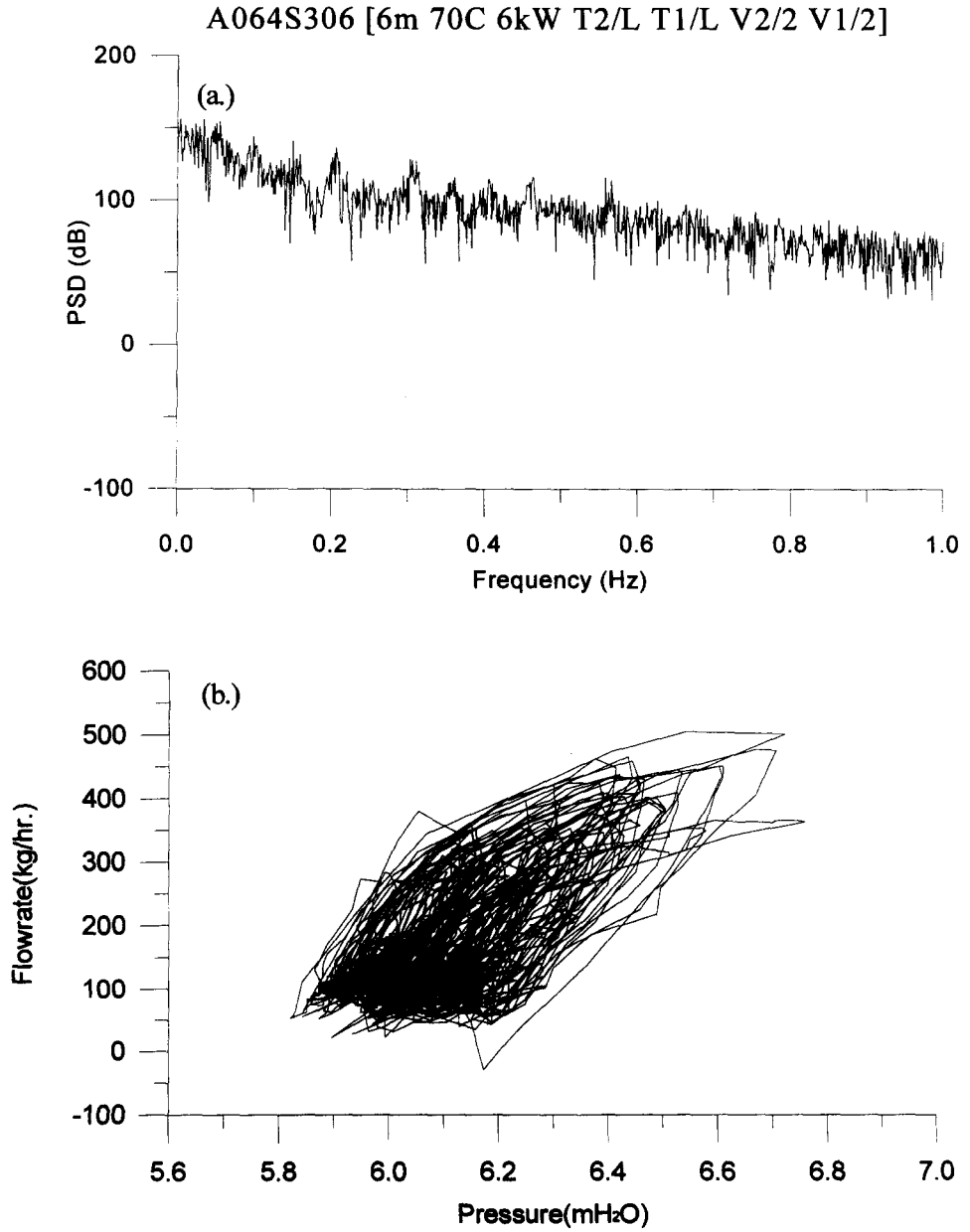

Figure 11. (a) Power spectrum of loop pressure. (b) Phase portrait in the plane of loop pressure and flow rate for a typical chaotic flow shown in figure 10.

As its name implies, chaotic flow has no order at all. Table 1 indicates that the peak flow rates for most chaotic flows are greater than 300 kg/h, and, unlike the other three modes of flow, the time percentage of each flow pattern for chaotic flow is quite sensitive to the operating conditions. The time percentage of single-phase flow and bubbly flow with a very low void fraction could be as high as 96% or as low as 57%. The ranges of time percentage for the bubbly flow with a medium to high void fraction, slug flow and churn flow are from 3 to 15, from 2 to 30, and from 0 to 14, respectively. Figure 10 displays the time evolutions of loop mass flow rate, riser fluid temperature, loop pressure and flow pattern in the upper and lower riser for a typical case of chaotic flow. All the time evolutions suggest that the oscillations are chaotic. This is further confirmed by the power spectrum of pressure and phase portrait of loop mass flow versus loop pressure shown in figure 11.

To further quantify this chaotic oscillation and confirm that it is indeed chaotic, the correlation dimension of the chaotic flow shown in figure 10 is evaluated based on the pseudo-phase-space of loop mass flow rate following the procedure given in Parker and Chua (1989) and Lahey (1992). The correlation dimension can be determined from the slope of $C(\epsilon)$, given by

$$C(\epsilon) = \lim_{n\to 0} \frac{1}{n^2} \sum_{i\neq j}^{n} \sum_{j=1}^{n} H(\epsilon - |x_i - x_j|)$$

where H is the Heaviside unit function and x_i (or x_j) is a point in D_b-dimensional trajectory produced from the time series of D_b variables formed by $w(t)$, $w(t+\tau)$, . . . , $w(t+(D_b-1)\tau)$. Here $w(t)$ is the loop mass flow rate and τ is the delay time. In the present study, $\tau = 5$ s is used. Figure 12 shows $C(\epsilon)$ in a log–log plot using the imbedding dimension D_b as a parameter. The slope changes insignificantly after $D_b = 7$. The slope of the least squares fitting straight line in $-19 \leqslant \log_2\epsilon \leqslant -14$ shown in figure 12 with $D_b \geqslant 7$ gives the correlation dimension of 2.88. This non-integral value of correlation dimension confirms that the oscillation shown in figure 10 is indeed chaotic.

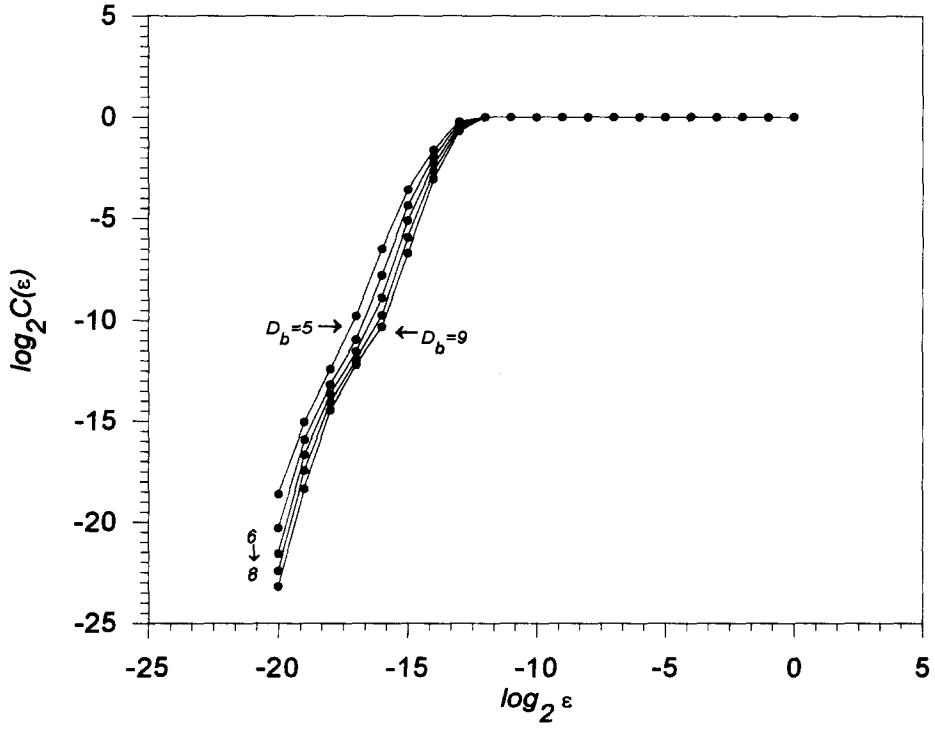

Figure 12. Representations of correlation dimension on the $\log_2 C(\epsilon)$–$\log_2\epsilon$ plane for the chaotic flow shown in figure 10.

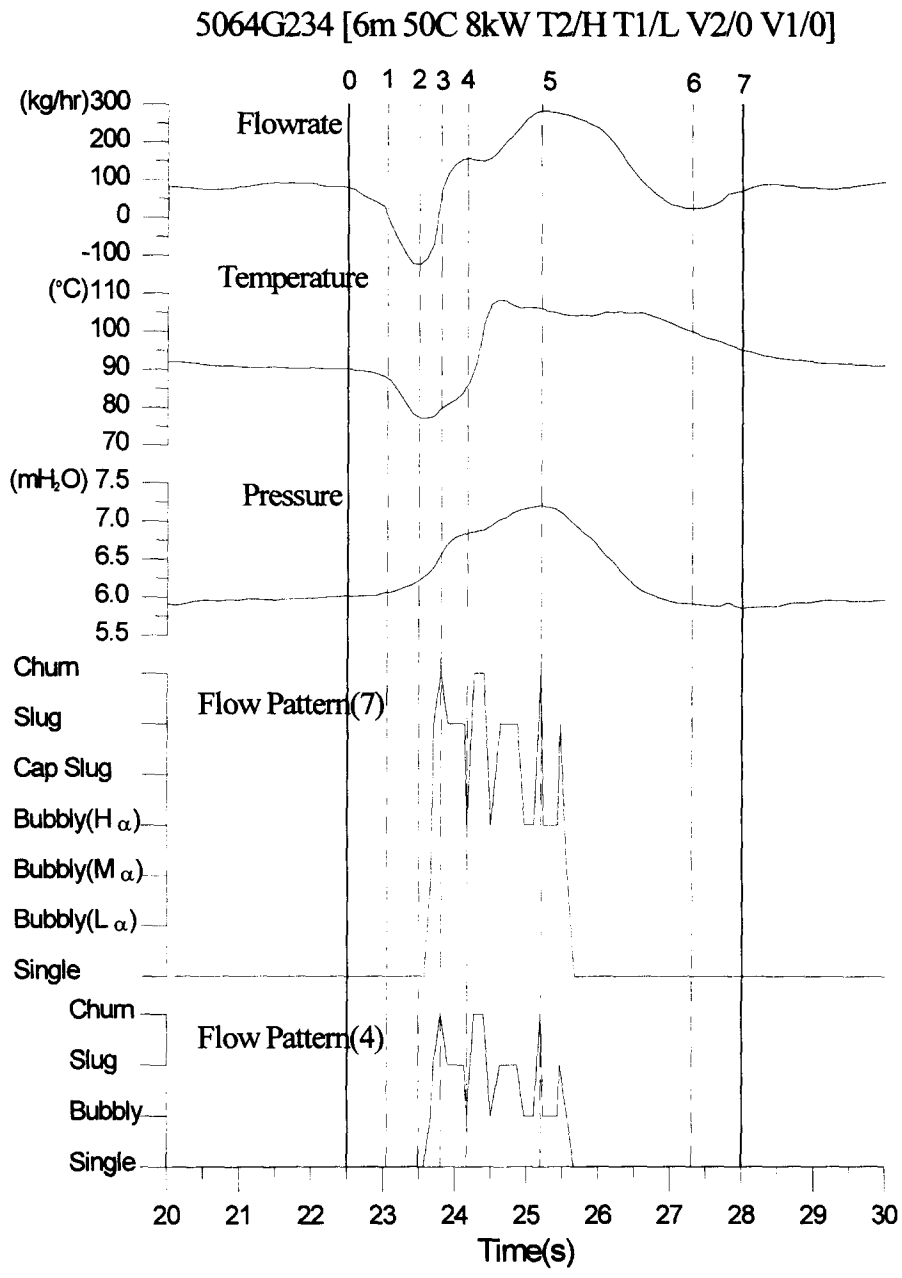

Figure 13. A zone look of a period of oscillation for periodic flow with a large magnitude.

4.2. *Change of flow pattern and flow mechanism*

The dynamic flow visualization of this study allows a detailed investigation into the mechanism of flow oscillation. Using the large magnitude oscillation during two-channel operation as an example, a zone look of a period of oscillation is given in figure 13. The corresponding flow patterns for several instant marked in figure 13 are displayed in figure 14. At point 1, which is at the end of a relatively long time of low flow rate, the flow pattern in the lower riser is mainly single-phase flow as shown in figure 14(a) or bubbly flow with a very low void fraction as shown in figure 14(b). Because the flow rate is relatively small, the fluid has enough time to be heated and boiled in the heated region. Direct visualization in the heated region indicates that bubbles were first generated in the region near the exit of heated region. This phenomenon lasts for a relatively long time and the fluid in the heated region then becomes saturated or near saturated and void generation in the

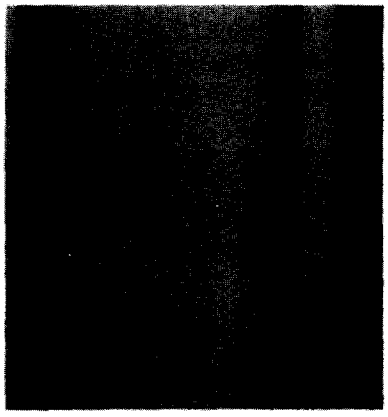

a. single phase flow
(Instant 0 in Fig.13)

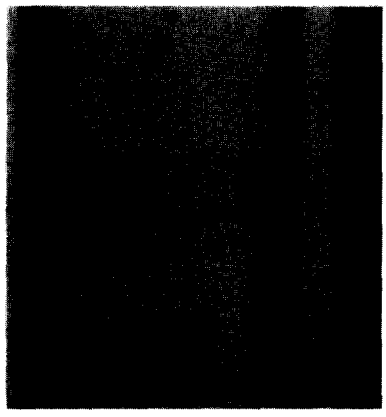

b. bubbly flow with a very small void fraction
(Instant 0 in Fig.13)

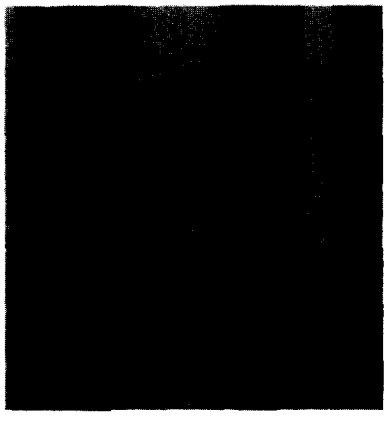

c. slug flow
(Between instants 2 and 3 in Fig.13)

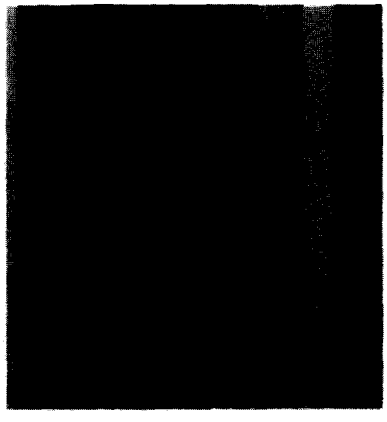

d. churn flow
(Instant 3 in Fig.13)

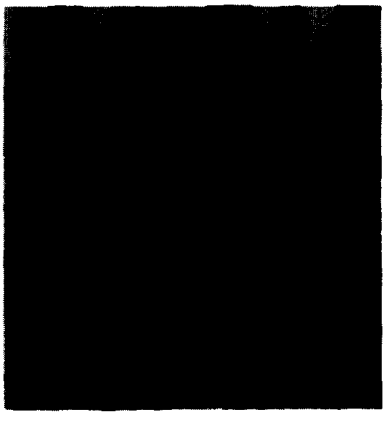

e. bubbly flow with a very high void fraction
(Instant 4 in Fig.13)

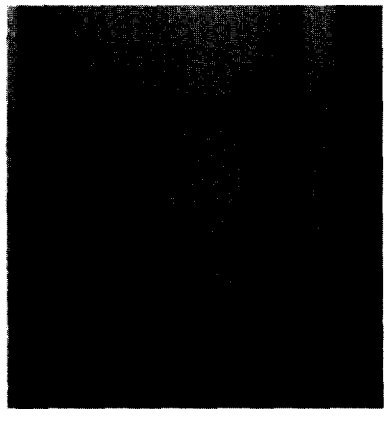

f. bubbly flow with a very small void fraction
(Instant 7 in Fig.13)

Figure 14. Flow patterns in the lower riser for various instants in figure 13.

heated region becomes very violent. The flow pattern in the heater region becomes a sort of annular flow and the liquid is expelled very quick in both upward and downward directions. Consequently, a reversed flow was recorded. Note that the flow meter is in the lower horizontal section and is

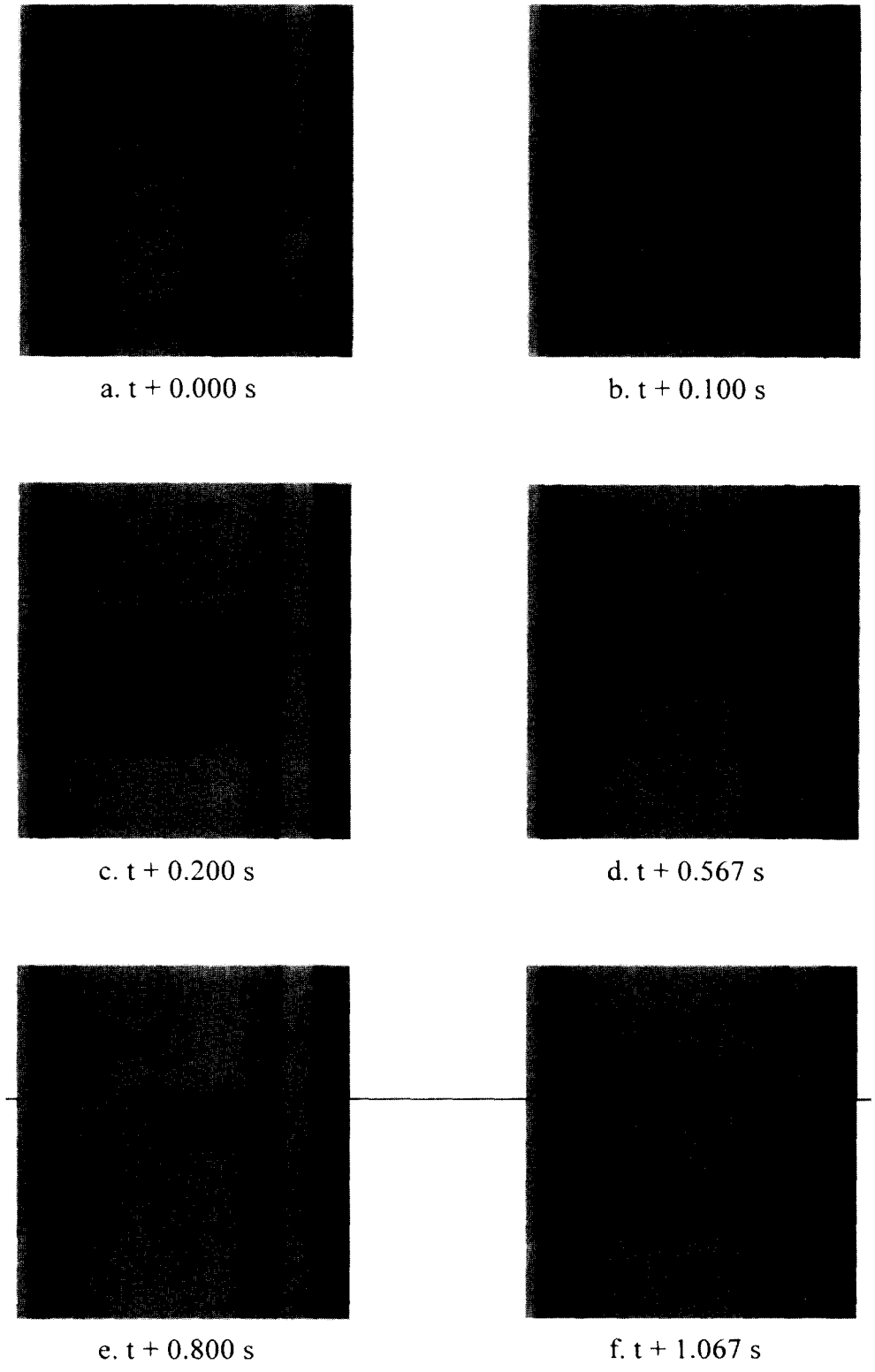

Figure 15. Flow patterns change in the lower riser during reversed flow similar to that from instant 5 to instant 6 in figure 13.

relatively close to the entrance of heated region. On the other hand, the cool fluid in the unheated channel is also forced, by the expelled liquid, to enter the riser region of the heated channel. As a result, the riser temperature in the heated temperature is decreasing during the flow reduction or flow reversed as shown in figure 13.

A great deal of void is generated during flow reduction and flow reversed period. The buoyancy force created by the void makes the flow become upward again and increase very rapidly. In the meantime, the voids in the heated region move upward to the riser and flow patterns there become slug flow, churn flow, and bubbly flow with a high void fraction, alternatively as shown in figure 14(c), (d) and (e), respectively. Such a large flow with fast changing flow pattern is followed by a relatively slow bubbly flow with a very small void fraction as shown in figure 14(f). Further discussion is given next.

The large flow rate in the loop introduces highly subcooled liquid from the downcomer into the heated region and sweeps the void away from the heated channel quickly. The buoyancy force created by the density difference between the heated channel and the unheated channel or between the heated channel and the condenser and downcomer region will be reduced or even reversed. Consequently, the loop flow rate is decreased or even reversed near the instant marked 6 in figure 13. Figure 15 is an evidence of this particular kind of reversed flow. The Taylor bubble in the riser is compressed to be shorter and shorter and moved downward further and further due to the reversed flow. Eventually, the Taylor bubble becomes a bubble more or less like an ellipsoid. In the interval between figure 15(d) and (e), i.e. $0.567 < t < 0.800$ s, the bubble is motionless indicating the flow is stagnant. After this still moment, the upward flow is resumed as suggested by figure 15(f). Since this kind of reversed flow is not very strong and starts near the exit of the heated channel, the flow meter at the lower horizontal section may not record the phenomenon for this case.

4.3. *Single factor effect*

The Taguchi method makes it possible to examine the effect of a single factor. Table 3 summarizes the effects of seven factors including the number of channels, inlet temperature, heating power, upper pressurizer, lower pressurizer and the loss coefficients due to control valves in the single-phase and two-phase regions, respectively, on various flow characteristics, including oscillation period, peak flow rate and time percentage of each flow pattern. The table clearly indicates that the number of channels (one or two), inlet temperature and heating power are the three most significant factors that influence the loop behavior, while the other four factors have only minor effects.

Table 3. Summary of single-factor effects based on the Taguchi orthogonal experimental matrix

Factor	Level	File name	Mode	Oscillation period (s)	Peak flow rate (kg/h)	Time percentage of each flow pattern in the lower riser (%)			
						Single phase	Bubbly flow	Slug flow	Churn flow
Double/ single	Double channel	5064G204	Periodic	~9.9	>300	78.9	4.3	9.9	6.9
	Single channel	5064G306	Periodic	~91	150–300	99.7	0.3	—	—
Inlet temp	60	5065G284	Periodic	~8.9	>300	76.7	7.1	11.1	5.1
(°C)	70	5065G294	Chaotic	—	>300	74.2	7.0	12.3	6.5
Heating power	6	50653244	Steady	—	<150	100	—	—	—
(kW)	7	5065F254	Steady	—	<150	100	—	—	—
Upper pressurizer	Low	5065L2A4	Periodic	~9.1	>300	80.2	8.2	7.3	4.3
(water level)	Disconnected	5065L2B4	Periodic	~13.0	>300	82.9	8.1	6.7	2.3
Lower pressurizer	High	5065L2C4	Periodic	~9.7	>300	78.9	9.5	8.1	3.5
(water level)	Low	5065L2D4	Periodic	~9.6	> 300	79.3	9.5	8.9	2.3
Two-phase flow valve	2 1/2	5064G224	Periodic	~9.6	>300	79.5	5.4	10.8	4.3
(turns of closure)	0	5064G234	Periodic	~10.1	>300	78.7	3.7	11.2	6.4
Single-phase flow valve	2 1/2	5065F264	Periodic	~10.0	>300	77.9	9.3	7.9	4.9
(turns of closure)	4 1/4	5065F274	Periodic	~10.2	>300	79.3	7.9	7.9	4.9

Reference experiment: 5064G204 [6 m 50°C 8 kW T2/H T1/L V2/4 V1/0].

The reference case, a double channel case with heating power of 8 kW, inlet temperature of 50°C and other factors listed in table 3 is characterized by a large magnitude oscillation with a peak flow rate greater than 300 kg/h. The oscillation period is 9.9 s. The total time percentage of slug and churn flows is 16.5%. When the unheated channel is closed and after the quasi-steady state under single-channel operation is reached, the flow becomes oscillation with a medium magnitude, i.e. with a peak flow rate between 150 and 300 kg/h. The oscillation period is almost 10-fold of that for the double channel case. Slug and churn flows totally disappear. This is consistent with the significant reduction in peak flow rate. The vanishing of the slug and churn flows suggests that the void fraction in the riser, and hence the buoyancy force, is relatively small. Thus, the peak flow rate is decreased. The oscillation period during double channel operation is primarily controlled by the circulation within the loop formed by the two parallel channels. That is to say, the fluid flows upward in the heated channel and a part of the fluid flows downward in the unheated channel. The flow path and resistance of this internal loop is much smaller than the outer loop, that is the sole flow path during single-channel operation. Consequently, the oscillation period during single-channel operation is much longer than that during double-channel operation.

As is well known, the inlet temperature or inlet subcooling, has a significant effect on two-phase natural circulation loop behavior. When the inlet temperature is increased from 50 to 60°C, the oscillation period is decreased by about 1 s and the time percentages of bubbly flow with a medium void fraction, and slug and churn flows are significantly increased. This time percentage is further increased and the flow becomes chaotic when the inlet temperature is further increased by 10°C.

The heating power is another very important factor affecting two-phase natural circulation loop behavior. When it is lowered to 7 or 6 kW, the oscillating flow is stabilized with the maximum flow rate less than 150 kg/h. Moreover, the flow pattern is dominated by single-phase or bubbly flow with a very low void fraction. Slug and churn flows disappear.

In the present study, the upper and lower pressurizer and the loss coefficients due to control valves in both single- and two-phase regions had only a minor effect on loop behavior. This is probably because the loop behavior during dual-channel operation is primarily controlled by the inner loop formed by the heated and unheated channel.

5. CONCLUSIONS

The present study develops dynamic image processing techniques based on gray level distribution to explore the correlation between two-phase flow patterns and other thermal hydraulic properties in a two-phase natural circulation loop. The following conclusions may be drawn from this study.

(1) There are four different modes of flow identified in the present study, namely, steady flow with a flow rate less than 150 kg/h, periodic flow with a medium magnitude (peak value from 150 to 300 kg/h), periodic flow with a large magnitude (peak value greater than 300 kg/h) and chaotic flow.

(2) Different flow patterns prevail in different modes of flow. For both the steady flow and periodic flow with a medium magnitude, single-phase flow and bubbly flow with a very small void fraction, each of which occurs about 50% of time, are the only two flow patterns present in the lower riser. For periodic flow with a large magnitude and chaotic flow, slug and churn flows become significant and induce large peak loop flow rates. The time percentage taken by these two flow patterns for periodic flow with a large magnitude is typically about 20–25%. For chaotic flow the time percentage of each flow pattern is quite sensitive to experimental conditions.

(3) Significant flashes take place in the riser and may influence the mode of flow. The periodic flow with a medium magnitude is induced by the flash effect.

(4) For the periodic flow with a large magnitude during double channel operation, the time percentage of both slug and churn flows decrease with increase in oscillation period.

(5) Simultaneous measurements of two-phase flow pattern and other thermal hydraulic properties enable detail investigation into loop flow mechanism.

(6) Single factor studies based on the Taguchi experimental matrix indicate that the number of channel, inlet subcooling and heating power are the three most important factors influencing two-phase flow pattern and other thermal hydraulic properties.

This experimental study indicates that dynamic variations of flow pattern and flashing effect play important roles for two-phase flow in a low pressure natural circulation loop. Incorporating such effects in future modeling works is needed to accurately predict the complex physical phenomena in the loop. The dynamic flow pattern data presented in this study would enhance our capability in modeling such important effects.

Acknowledgements—This work was supported by the National Science Council of the Republic of China under Contract No. NSC85-2212-E007-093. The authors would like to express their appreciation to Mr J. D. Lee for his evaluating the correlation dimension for the chaotic flow and plotting figure 12.

REFERENCES

Aritomi, M., Chiang, J. H. and Mori, M. (1992) Fundamental studies on safety-related thermo-hydraulics of natural circulation boiling parallel channel flow systems under startup conditions (mechanism of Geysering in parallel channels). *Nuclear Safety* **33,** 170–182.

Chexal, V. K. and Bergles, A. E. (1973) Two-phase instabilities in a low pressure natural circulation loop. *AIChE Symp. Ser.* **69,** 37–45.

Delmastro, D. F., Clausse, A. and Converti, I. (1991) The influence of gravity on the stability of boiling flows. *Nuclear Engineering and Design* **127,** 129–139.

Fairholm, W. H., Harvel, G. D., Campeau, J. C. and Chang, J. S. (1991) Visualization of two-phase interfaces in a natural circulation loop by a real-time neutron radiography imaging system, *Proc. Nat. Heat Transfer Conference*, Minneapolis, Minnesota, 28–31 July 1991, pp. 199–206. American Nuclear Society.

Fukuba, K. and Kobori, T. (1979) Classification of a two-phase flow stability by density wave oscillation model. *J. Nuclear Science and Technology* **16,** 95–108.

Jain, K. C., Petrick, M., Miller, D. and Bankoff, S. G. (1966) Self-sustained hydrodynamic oscillations in a natural circulation boiling water loop. *Nuclear Engineering and Design* **4,** 233–252.

Kyung, I. S. and Lee, S. Y. (1994) Experimental observation on flow characteristics in an open two-phase natural circulation loop. *Nuclear Engineering and Design* **159,** 163–176.

Lahey, Jr, R. T. (1992) Application of fractal and chaos theory in the field of multiphase flow and heat transfer. In *Boiling Heat Transfer, Modern Developments and Advances*, ed. R. T. Lahey, Jr, pp. 317–318, Elsevier, Amsterdam.

Lee, S. Y. and Ishii, M. (1990) Characteristics of two-phase natural circulation in freon-113 boiling loop. *Nuclear Engineering and Design* **121,** 69–81.

Misawa, M. and Anghaie, S. (1991) Zero-gravity void fraction and pressure drop in a boiling channel. *AIChE Symp. Series* **87,** 226–235.

Parker, T. S. and Chua, L. O. (1989) *Practical Numerical Algorithms for Chaotic Systems*. Springer, New York.

Hsieh, C. C. (1996) Two-phase flow patterns in a natural circulation loop. M.S. thesis, Department of Nuclear Engineering and Engineering Physics, National Tsing Hua University, Hsinchu, Taiwan. (In Chinese.)

Wu, C. Y., Wang, S. B. and Pan, C. (1996) Chaotic oscillation in a low pressure two-phase natural circulation loop under low power and high inlet subcooling conditions. *Nuclear Engineering and Design* **162,** 223–232.